JOURNAL OF PROPULSION AND POWER
Vol. 15, No. 3, May–June 1999

Free-Flight Experiment and Numerical Simulation for Cold Thruster Plume

M. S. Ivanov* and G. N. Markelov†
Institute of Theoretical and Applied Mechanics, 630090, Novosibirsk, Russia
Yu. I. Gerasimov,‡ A. N. Krylov,‡ and L. V. Mishina‡
RSC "ENERGIA," 141070, Korolev, Moscow Region, Russia
and
E. I. Sokolov§
Institute of High Performance Computing and Data Bases, 194291, St. Petersburg, Russia

An experiment, Astra-2, was performed at the space station Mir in 1995–1996 to study its ambient atmosphere parameters. For far-field plume research, the equipment of Astra-2 included a small cold gas thruster using a marked gas, argon. The results of this research offer a good basis for validation of various numerical approaches for plume flows, from simple engineering models to exact numerical approaches using a Navier–Stokes solver in the continuum regime and a direct simulation Monte-Carlo code in the near-continuum, transitional, and free-molecular regimes. A comparison of experimental and numerical results shows the necessity of accounting for argon condensation processes in the nozzle and in the vicinity near the nozzle.

Nomenclature

B	=	breakdown parameter, $M\sqrt{[(\pi\gamma/8)](\lambda/\rho)\lvert d\rho/ds\rvert}$
F	=	nozzle exit area/throat area ratio, $(r_e/r_*)^2$
I	=	specific momentum
M	=	Mach number
N	=	mass flow rate
n	=	numerical density
p	=	pressure, Pa
R	=	gas constant
r	=	radius
S	=	molecular speed ratio
s	=	distance along streamline
T	=	temperature, K
U	=	velocity, m/s
u	=	velocity
β	=	reciprocal of the most probable molecular speed in an equilibrium gas, $1/\sqrt{(2RT)}$
γ	=	specific heat ratio
θ	=	angle between plume axis and point of interest
λ	=	mean free path
ξ	=	molecular velocity
ρ	=	mass density, kg/m^3

Subscripts

e	=	nozzle exit condition
l	=	limiting value
w	=	nozzle wall
x, y, z	=	coordinate axis
0	=	stagnation chamber condition
$*$	=	sonic condition
$\perp$	=	perpendicular (to flow velocity)
$\parallel$	=	parallel (to flow velocity)

Presented as Paper 98-0898 at the AIAA 36th Aerospace Sciences Meeting, Reno, NV, Jan. 12–15, 1998; received Feb. 4, 1998; revision received July 24, 1998; accepted for publication Sept. 15, 1998. Copyright © 1998 by the American Institute of Aeronautics and Astronautics, Inc. All rights reserved.

*Head of Computational Aerodynamics Laboratory, 4/1 Institutskaya St. Senior Member AIAA.
†Research Scientist, Computational Aerodynamics Laboratory, 4/1 Institutskaya St.
‡Research Scientist, Aerothermodynamic Department.
§Head of CFD Laboratory, P.O. Box 71. Senior Member AIAA.

Introduction

ONE of the specific features of spacecraft functioning at low Earth orbit is the creation of its own ambient atmosphere (OAA) that envelopes the spacecraft. This OAA differs from the surrounding space vacuum by possessing a larger pressure and density, by a variety of chemical compositions of gaseous components, and by the presence of liquid and solid particles. In some cases, the OAA can exert a significant, often adverse, effect on the operation of service systems, onboard scientific equipment, and the interpretation of results of onboard scientific research. One of the main sources for creating a spacecraft OAA is the reaction control system (RCS) that uses a series of thrusters. Under the conditions of high vacuum, the products of fuel combustion in these thrusters can turn up to 180 deg and involve a background pressure increase of several orders of magnitude. The ground-based research of the processes at the periphery of thruster plumes is rather complicated because it is difficult to ensure high vacuum and simultaneously to reproduce the full-scale parameters—namely, the nozzle pressure ratio, the Mach and Reynolds numbers at the thruster exit, etc. These parameters determine the thruster plume effect on the spacecraft OAA, as well as their force, thermal, and contaminating loads on spacecraft elements. The problem of OAA parameters of orbital spacecraft was of great interest more than two decades ago, almost simultaneously in Russia and the United States. It is significant that scientists of both countries dealing with this problem came to the same conclusion in the mid-1970s: successful investigation of the OAA cannot be performed without proper full-scale research of the orbital flight of a spacecraft. A step forward in OAA research was the experiment called Astra-2, which was performed in 1995–1996 on the space station Mir. Among many other instruments, the equipment of Astra-2 included a small cold gas thruster using a marked gas, argon. The measurements were performed in the far field of the plume and particularly in its peripheral region.

The numerical study of the rapidly expanding plume exhaust flow requires a special approach to be used to obtain physically reliable solutions. This is mainly because the entire range of flow regimes is observed, from the continuum flow within the nozzle and near vicinity through the transitional to free-molecular flow at large distances from the nozzle. The simulations must be performed for very

Table 1 Experimental conditions

Case	Date	Time	$p_0 \times 10^{-5}$	T_0	Tw	θ
1	1-30-96	18.53.01	10.22	298	302	From +135 deg to +35 deg and back to +135 deg
2	6-2-96	20.31.13	10.44	299.4	305.8	From −6 deg to +122 deg
3	6-2-96	21.56.53	10.56	285.7	294.5	From −4.5 deg to +123 deg

large spatial scales (hundreds or thousands of nozzle diameters) to examine, in detail, the flow within the nozzle as well as the far-field regions.

A special combined multizone approach[1] is used in the present paper to accurately predict these flows. In fact, the plume flow is divided into three zones according to the rarefaction degree, and the solution is obtained using different numerical approaches in different zones.

In the first zone, the Navier–Stokes equations are solved; then, when the rarefaction becomes significant and the Navier–Stokes equations are no longer valid, the direct simulation Monte Carlo (DSMC) method is applied. Finally, in the third zone, where the free-molecular flow occurs, the test particle Monte Carlo (TPMC) method[2] can be used. The DSMC method requires the heaviest computational effort and is the kernel connecting the continuum and free-molecular regions.

In practical applications that require an estimation of the plume far-field region, various engineering models based on both the continuum and free-molecular approaches are frequently used.[3–5]

The main objectives of the present paper are as follows:

1) Conduct preliminary analysis of experimental data for a model argon thruster.

2) Perform numerical simulations of the plume flow inside the nozzle, its near vicinity, and far field up to the distance of 800 nozzle diameters.

3) Assess the applicability of various engineering plume models.

4) Provide comparisons of numerical and experimental data on the angular distribution of relative pressure in the plume far field (about 800 nozzle diameters).

Experimental Setup

The OAA and thruster plume have been experimentally studied using the Astra-2 equipment. It allows for extensive measurements of pressure, gas composition, and contamination in a considerable volume around the spacecraft, including regions a distance of 2 m from the spacecraft surface (as well as the near-surface zone). The study of distant zones was possible as a result of the positioning of the measurement system containing a pressure gauge and mass spectrometer, mounted on a moving bar. The bar is about 2 m long and can deflect up to 135 deg from the surface.

A model thruster operating with a marked gas (argon) was placed at the bar foot. It consisted of three main elements: 1) control system, 2) micronozzle, and 3) two tanks filled with argon and the pneumatic hydrosystem for supplying the latter to the nozzle in three flow rates: gasdynamic (1 g/s, 0.5 g/s) and effusion (10^{-3} g/s).

The micronozzle has the following parameters: half-angle= 10 deg and nozzle exit area/throat area ratio $F = 18.8$.

The measurement system, model thruster, and moving bar were installed outside of the Spektr module of the space station Mir. A photograph of the bar with the measurement system at its maximum deflection from the surface is presented in Fig. 1.

The pressure gauge installation and a bar position with respect to the nozzle axis of the model thruster are shown in Fig. 2. The accuracy of the nozzle-axis orientation toward the measurement system center was better than 1.5 deg for a bar deflection angle of 135 deg, the angle between the scanning plane and direction toward the gauge was 4.2 deg, the relative distance to the measurement point was $r/r_e = 1608.7$, and the angular velocity of the bar motion was 2.5 deg s^{-1}.

The pressure was measured by an ionic pressure gauge, PMI-45M, with a measurement range from 10^{-5} to 1.0 Pa, calibrated with nitrogen. The pressure-gauge sampling rate was 50 Hz, and the

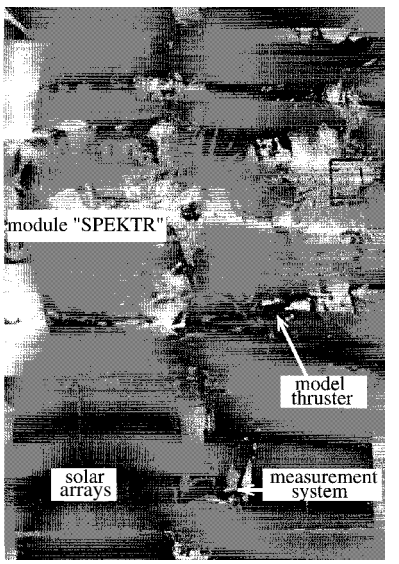

Fig. 1 Astra-2 equipment photograph taken by the crew of the Space Shuttle during its undocking with space station Mir in STS-81. (Courtesy NASA.)

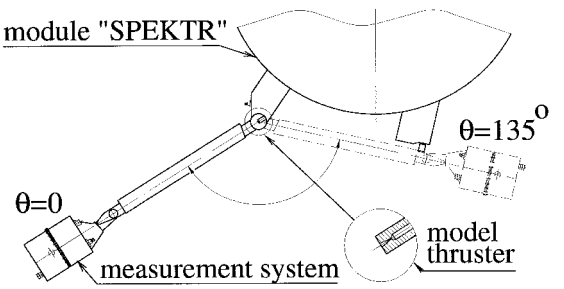

Fig. 2 Sketch of bar attachment.

sampling rate of the bar-angle gauge was 0.77 Hz. During processing, the data on the angular position of the bar were reconstructed by linear interpolation.

In this paper, experimental and numerical data are presented for the flow rate of 1 g/s. The conditions of measurements are listed in Table 1. The angular pressure distribution in the far field of the plume ($r/r_e = 1608$) is shown in Fig. 3 in a relative form, i.e., $p(\theta)/p(\theta = 0)$. This is primarily connected with the fact that a thorough analysis of rarefied flow around and inside the pressure gauge is necessary for calculating the pressure gauge data because the gauge axis has a direction of 4.2 deg with respect to the scanning plane; i.e., the flow inside the gauge is essentially three dimensional.

Only preliminary comparisons of the relative pressure are currently possible. Even so, one has to assume that the influence of the preceding effects (rarefaction, three-dimensional flow, etc.) are independent of the angle θ.

Note that three experimental runs performed at different times with different attitudes of the orbital station Mir are in fairly good agreement.

Numerical Approach

The combined multizone approach implies that the flowfield is partitioned into several zones. The flow in the first zone, within

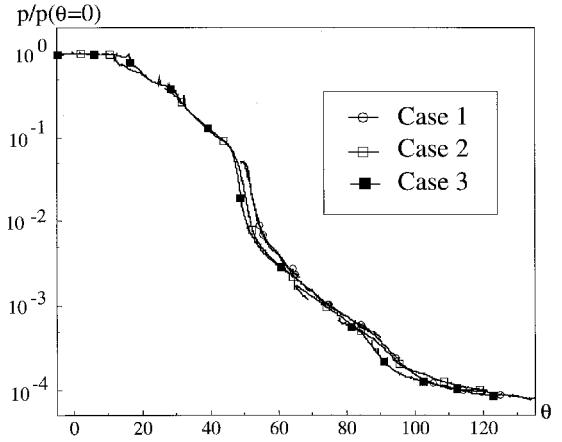

Fig. 3 Angular distribution of relative pressure in the plume far field (r/r_e = 1608).

the nozzle and near vicinity, was computed using a finite volume Navier–Stokes code.

A high-resolution essentially non-oscillatory (ENO) scheme of third order was used for the spatial approximation of inviscid terms of the Navier–Stokes equations, whereas viscous terms were calculated with second-order central differencing. The time advancement was completed with the fractional step method using splitting on physical processes. During the first fractional step, the solution was governed by the inviscid equations and all viscous terms were put to zero. The obtained solution for density was ultimate, but all other gasdynamic quantities changed in the second fractional step when only viscous terms of the system were taken into account. This fractional step was performed with a backward Euler implicit scheme to increase the available time increment and to accelerate convergence to a steady solution. The diagonal approximation of the viscous Jacobian was used when evaluating the implicit terms of the equations.

Results of the Navier–Stokes computations were used as incoming flow conditions for the second zone, which was computed with a DSMC code. The location of the boundary between the Navier–Stokes and DSMC regions is based on the condition that the breakdown parameter B[4] not be greater than 0.05. The DSMC region propagates the flow domain until the flow becomes free molecular. The DSMC method applied was an axisymmetric formulation. This is the principal method used to describe flows where both rarefaction and viscous effects are significant. The majorant frequency scheme of the DSMC method with coupling free-cell and cell algorithms was used.[6] A variable hard sphere model[7] with an exponent of 0.81 for viscosity-temperature dependence was chosen as a potential for intermolecular collision. The particle reflection on the body surface was modeled according to the diffuse law with complete accommodation of energy.

The second zone (DSMC region) is divided into a set of subdomains, where the local Knudsen number varies by no more than one order of magnitude along the plume axis. The specific time step and molecular weight (ratio of the number of real molecules to the number of model molecules) are employed in each subdomain. These subdomains are computed sequentially, and the parameters on the downstream boundary of a subdomain are used as the input data at the upstream boundary of the next subdomain. An important feature of the approach is the use of an ellipsoidal distribution function:

$$f = \frac{n}{\sqrt{T_x T_y T_z}(2\pi R)^{\frac{3}{2}}} \exp\left[-\frac{(\xi_x - u_x)^2}{2RT_x} - \frac{(\xi_y - u_y)^2}{2RT_y} - \frac{(\xi_z - u_z)^2}{2RT_z} \right]$$

This allows one to take into account the flow nonuniformity and to maintain nonequilibrium when simulating the injected molecules. The ellipsoidal distribution function reduces to Maxwellian in the case of Navier–Stokes/DSMC coupling.

The following engineering models for the plume are used:

1) RSC "Energia" model[3]:

$$\rho(0) = \frac{\rho_0 A(\gamma - 1)^{0.5}}{\left[(r/r_e)^2 F \theta_+^2\right]}$$

angular dependence

$$\rho(\theta) = \rho(0) \exp\left[-0.5(\theta/\theta_+)^2\right]$$

where r is the radius of the point of interest, and θ_+ is the characteristic angle:

$$\theta_+ = \operatorname{arctg}\sqrt{(1 - I)/I}, \qquad A = 8^{-0.5}[2/(\gamma + 1)]^{(\gamma + 1)/[2(\gamma - 1)]}$$

$$I = \left(1 + \frac{1}{\gamma M_e^2}\right)\left[1 + \frac{2}{(\gamma - 1)M_e^2}\right]^{-0.5}$$

2) Model[4]:

$$\rho(\theta) = \rho_* A(r_*/r)^2 f(\theta)$$

where $f(\theta) = \cos(\theta)^{2/(\gamma - 1)}$

$$A = \frac{U_*/2U_l}{\int_0^{\theta_l} f(\theta)\sin(\theta)\,\mathrm{d}\theta}$$

θ_l is the limiting turning angle of the gas at the nozzle exit, U_l is the limiting velocity of the gas $U_l = \sqrt{[(\gamma + 1)/(\gamma - 1)]}U_*$.

3) Symmetrical free-molecular source model[8]:

$$\rho(\theta) = \left(\frac{\beta N}{2\pi\sqrt{\pi r^2}}\right)\exp(-S'^2)\left[\exp(-\bar{S}^2) + \sqrt{\pi}\bar{S}(1 + \operatorname{erf}\bar{S})\right]$$

where $S' = S\sin\theta$, $\bar{S} = S\cos\theta$.

4) Asymmetrical free-molecular source model[5]:

$$\rho(\theta) = (\beta N \cos\Theta/A\pi r^2)\exp(-S'^2)\left[\exp(-\bar{S}^2) + \sqrt{\pi}\bar{S}(1 + \operatorname{erf}\bar{S})\right]$$

where $S' = S\sin\theta$, $\bar{S} = S\cos\theta$, Θ is the angle between the point of interest and the normal to a surface element

$$A = \exp[-(S\cos\alpha)^2] + \sqrt{\pi}S\cos\alpha[1 + \operatorname{erf}(S\cos\alpha)]$$

α is the angle between the flow velocity and the normal to a surface element.

Results

Nozzle Flow

The flow within the nozzle contains sub-, trans-, and supersonic parts, and was predicted by a Navier–Stokes solver. The Reynolds number based on the sonic parameters and throat radius is 4×10^4. Nevertheless, velocity slip and temperature jump conditions[9] with accommodation coefficients equal to unity were used on the nozzle wall, because the proper boundary conditions can considerably affect the expansion flow near the nozzle lip.

The Mach number contours inside the nozzle are shown in Fig. 4. The formation of an expansion fan in the beginning of the supersonic conical part of the nozzle can be distinguished. Being reflected on the nozzle axis and its wall, this fan leads to nonuniform flow in the nozzle exit plane. This nozzle forms a hypersonic flow, whose velocity is smaller by only 5% than the thermodynamic limit.

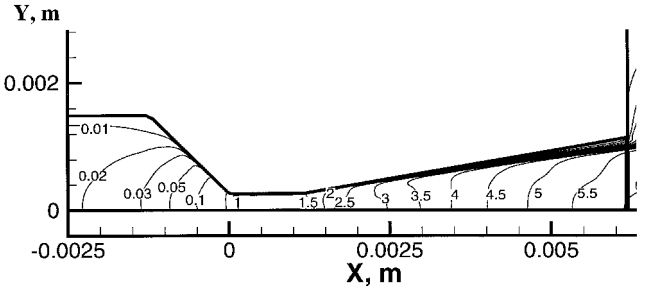

Fig. 4 Mach number contours inside the nozzle.

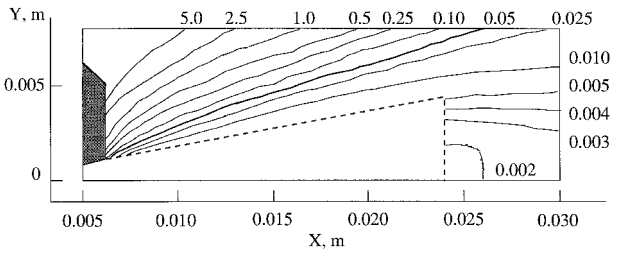

Fig. 5 Breakdown parameter contours in the plume near field (shaded area is a portion of the nozzle wall).

Flow in the Near Vicinity of Nozzle Exit

The flow near the nozzle lip is known to be characterized by a fast radial expansion of the flow, which rapidly becomes rather rarefied, and the Navier–Stokes equations are no longer applicable. A continuum description of the flow, however, can be used at large distances along the axis.

In the present experiment, the flow calculation in the near vicinity is complicated by the fact that the nozzle is located inside a cylinder, whose external wall radius is about $5r_e$. The flow interaction with the cylinder wall affects the back and side regions of plume flows.

The DSMC zone in the present work, therefore, starts immediately from the nozzle exit. The conical surface formed by the dashed line rotation (Fig. 5) was used as a starting surface for DSMC code. The flow properties along this surface are determined from the Navier–Stokes computation and used to characterize the molecules injected into the DSMC zone.

Figure 5 shows the breakdown parameter contours calculated by the DSMC code. In the streamwise direction, the breakdown contour ($B = 0.05$) extends rather far downstream. In the crossflow direction, however, the parameter B increases to 0.05 near the nozzle lip because of rapid expansion.

To analyze the accuracy of conjunction between the Navier–Stokes and DSMC approaches, the computation in the near vicinity of the nozzle exit was performed for overlapped computational Navier–Stokes and DSMC domains. Excellent agreement of density isolines is observed for both numerical methods (Fig. 6), except for the vicinity of the external nozzle wall.

The influence of this wall is even more substantial for the Mach number contours (Fig. 7). It is important to take this into account because this flow region is responsible for a formation of the plume far field at large values of θ.

The good agreement of core-flow parameters obtained by both approaches shows that it is not necessary to choose a breakdown parameter isosurface equal, for example, to 0.05 (see Ref. 10) to start the DSMC calculation. Such a surface often has a fairly complicated shape and, as a consequence, would require a complicated bridging of different computational grids. Meanwhile, the use of a simple-shaped starting surface with a variable breakdown parameter that does not exceeds 0.05 allows considerable simplification of the bridging of different grids. In this case, the modeling of near-continuum flows in a small vicinity of the starting surface does not cause any noticeable difficulty.

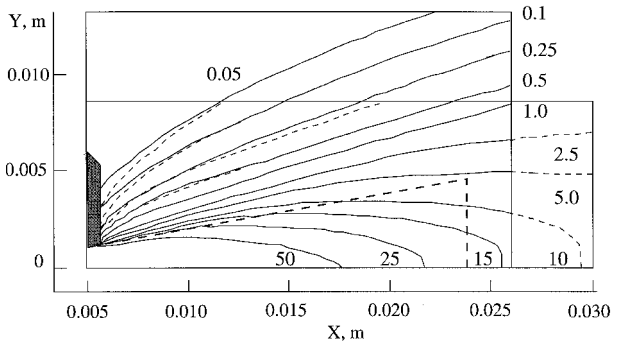

Fig. 6 Density contours: ——, Navier–Stokes solver; ----, DSMC code; shaded area is a portion of the nozzle wall; and rectangles are boundaries of Navier–Stokes and DSMC domains. Labels in unit of 10^{-3} kg/m^{-3}.

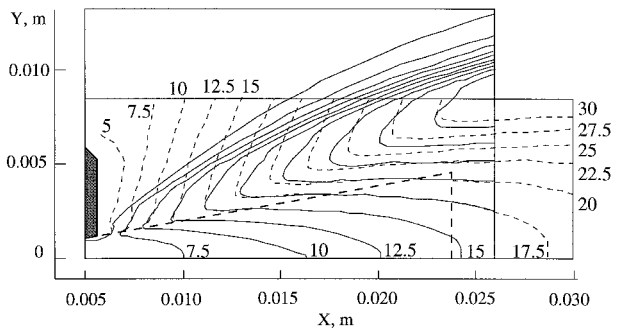

Fig. 7 Mach number contours: ——, Navier–Stokes solver; ----, DSMC code; shaded area is a portion of the nozzle wall; and rectangles are boundaries of Navier–Stokes and DSMC domains.

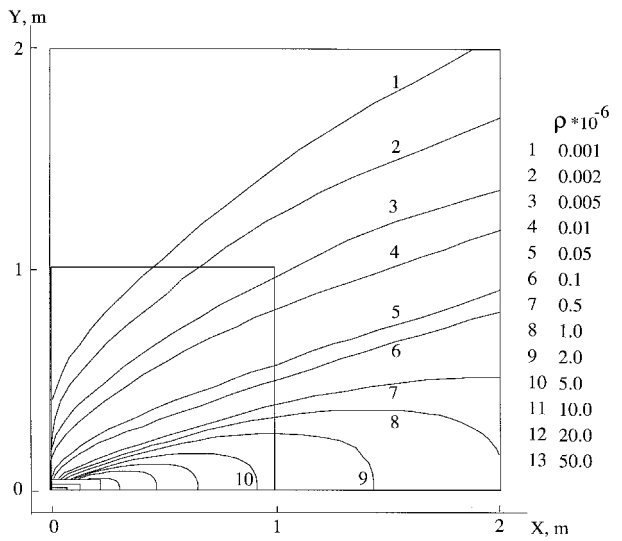

Fig. 8 Density isolines in the entire domain (rectangles are boundaries of DSMC subdomains).

Plume Far Field

The DSMC computational domain (zone) consisted of seven nested subdomains. The three largest subdomains are presented in Fig. 8 along with the density flowfield. The first four subdomains are not visible in the full-scale picture. About 10^6 model particles and 3×10^5–4×10^5 collisional cells were used in each subdomain, and the Knudsen number varied by less than a factor of 10 within each subdomain.

Because the main interest of this work is focused on computing the angular distribution of parameters in the far field, the behavior of streamlines is important for understanding the flow structure.

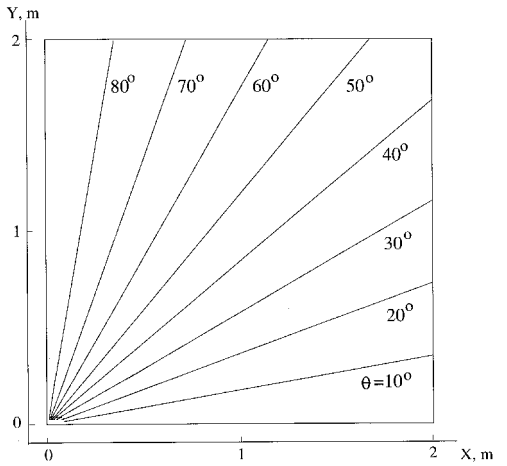

Fig. 9 Selected streamlines in the plume far field (DSMC code).

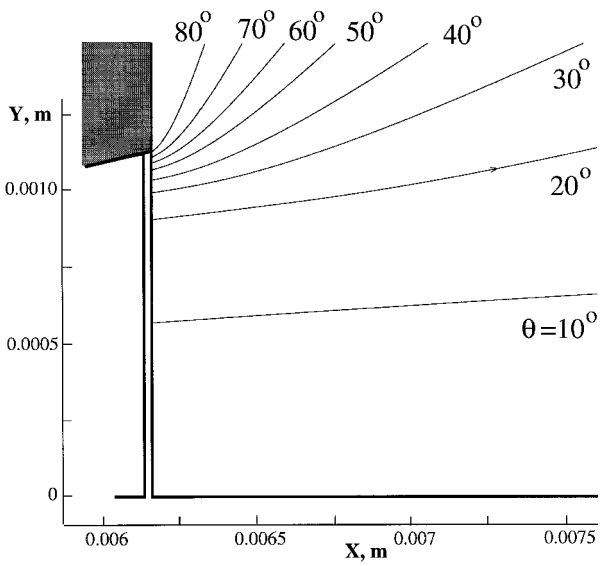

Fig. 10 Selected streamlines in the vicinity of the nozzle exit plane (Navier–Stokes solver, shaded area is a portion of the nozzle wall).

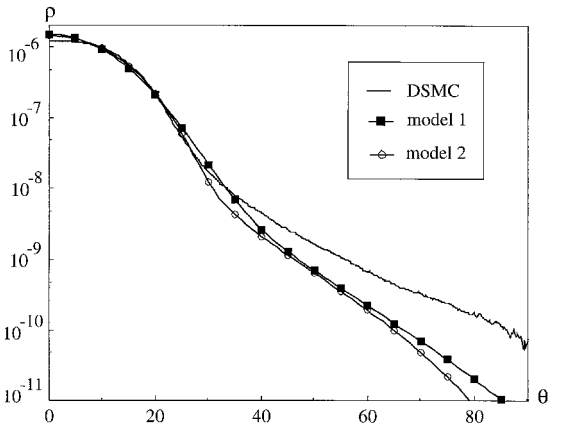

Fig. 11 Angular distribution of density in the plume far field (model starting line goes along the nozzle exit radius).

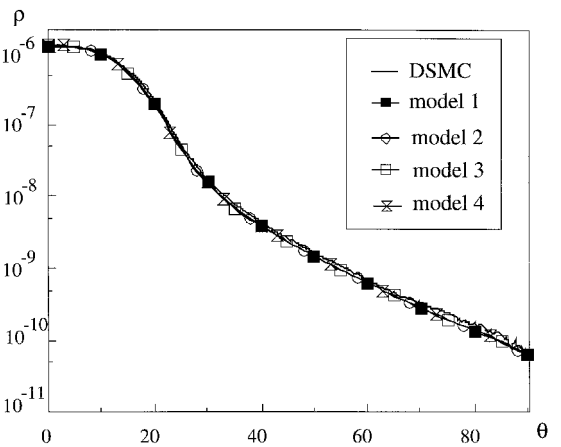

Fig. 12 Angular distribution of density in the plume far field (model starting line is the boundary of the first DSMC subdomain).

Figure 9 shows the streamline pattern, and Fig. 10 illustrates their behavior in the near vicinity of the nozzle exit. It is clearly seen that the streamlines are almost straight in the plume far field. Hence, a radial flow is observed in this region, and the flow center is in the nozzle exit plane. The flow structure rearrangement, from conical inside the nozzle to radial in the plume far field, occurs in the region extended a distance of about 10 nozzle diameters downstream of the nozzle exit plane. Note that the streamlines with angles larger than 30 deg originate at the boundary layer of the nozzle. Thus, the peripheral part of the plume flowfield is completely determined by parameters inside the nozzle boundary layer.

It is well known that the use of engineering models 1 and 2 based on the continuum approach does not allow one to predict directly the peripheral part of the plume without additional assumptions on the boundary-layer parameters. Therefore, in this paper, the distributed point-source models with variable governing parameters have been used along a certain line, where these parameters are known either from the numerical solution of Navier–Stokes equations or DSMC simulation. Thus, the final results calculated with these models are a superposition of contributions from many sources along the model starting line.

The angular distribution of density at the radius $r/r_e = 1608$ is presented in Fig. 11, which shows the DSMC computation results and the data obtained using continuum models 1 and 2. The model starting line was chosen along the nozzle exit radius, and the governing parameters for these models were obtained from the solution of Navier–Stokes equations. It is seen that these two models are in agreement, but overpredict the DSMC density value at the plume axis (20%) and underpredict it at the plume periphery (up to one order). The use of the model starting line along the outer boundary of the first subdomain of the second (DSMC) zone yields an excellent agreement between these models and DSMC results (Fig. 12). In addition, Fig. 12 also shows the data obtained using free-molecular models 3 and 4 that also predict successfully the angular density distribution in the far field of the plume.

A good agreement between the continuum models (1, 2), free-molecular models (3, 4), and DSMC results can be explained as follows. The bulk velocity at the boundary of the first subdomain of the second zone is already close to its thermodynamic limit. The density change is, therefore, determined in accordance with the continuity equation and the expansion geometry, and is practically independent of the local collisional frequency.

Intermolecular collisions within the plume have, however, a visible effect on the temperature behavior. Figure 13 shows the variation of the total (T), parallel ($T_\parallel$), and perpendicular ($T_\perp$) temperatures along the plume axis. The temperature $T_\perp$, which characterizes the scatter of molecular velocities in the direction perpendicular to the bulk gas motion, decreases faster than the total temperature. The temperature $T_\parallel$, that characterizes the scatter of molecular velocities in the gas flow direction, decreases considerably slower than the total temperature. This behavior of the total, parallel, and perpendicular temperatures is typical of the transitional flow regime, and the temperature splitting indicates the applicability limit of the continuum

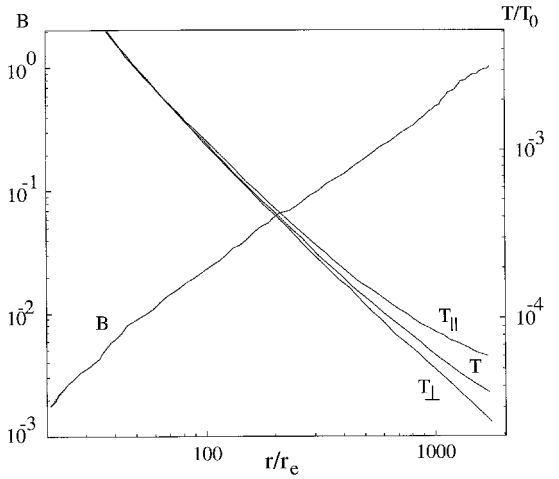

Fig. 13 Parameters along the plume axis.

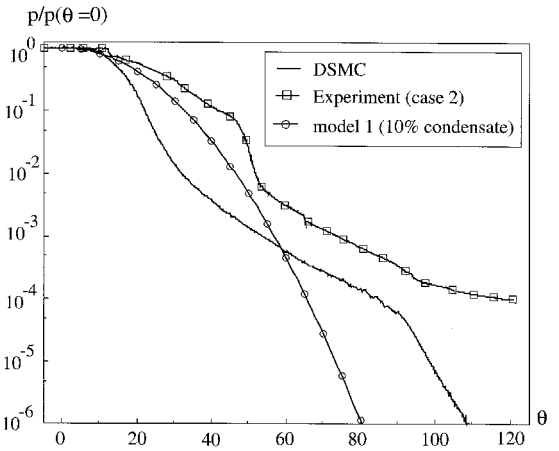

Fig. 14 Comparison of numerical and experimental angular distributions of relative pressure in the plume far field (r/r_e = 1608).

approach. Another criterion determining the applicability limit of the continuum approach is the magnitude of the breakdown parameter $B \approx 0.05$. The breakdown parameter variation along the plume axis is presented in Fig. 13. For $r/r_e = 90$ its value is $B = 0.02$, which is in agreement with the beginning of temperature splitting; i.e., this splitting starts somewhat earlier than when the parameter B acquires the value of 0.05.

Using the parameter B also as a criterion for determining the boundary between the transitional and free-molecular regimes, it is obvious that its value should be larger than unity. For example, along the plume axis at a large distance ($r/r_e = 1608$, see Fig. 14) B is about 1, but a complete freezing of $T_\parallel$ has not occurred, which would correspond to the free-molecular flow regime.

Comparison with Experiment

As noted earlier, only experimental data of the angular distribution of the relative pressure $p(\theta)/p(\theta = 0)$ are currently available. Figure 14 shows a comparison of experimental and calculated angular distributions of relative pressure for $r/r_e = 1608$.

It is clearly seen that the core flow in the DSMC results is twice as narrow as in the experiment (25 deg, DSMC; 50 deg, experiment). Such a considerable difference is apparently related to argon condensation, both inside the nozzle and in the near vicinity. The condensation results in a reduction of the relative plume momentum caused by heat release, and yields a substantial expansion of the plume core flow. The process of condensation has not been considered in the present work when solving the Navier–Stokes equations. A simple one-dimensional analysis[¶] of the nozzle flow with regard for condensation estimates the fraction of condensate to be about 10%. The point-source model 1 allows one to take into account condensation[3] through the decrease in relative plume momentum, I. The results for this model shown in Fig. 14 manifests a better agreement with experimental results. Obviously, the process of gas condensation continues in the near-vicinity region. Thus, for conditions of the Astra-2 experiment, the numerical analysis should also incorporate the condensation process both inside the nozzle and in the near vicinity.

The slope of numerical and experimental data in the plume periphery ($50 \le \theta \le 90$ deg) is identical. It can be explained by the fact that condensation is negligible in the nozzle boundary layer. For larger angles ($\theta \ge 90$ deg), the significant difference in the slope of experimental and numerical curves is observed. It is connected with the following fact. As seen from Fig. 2, at angles $\theta \ge 90$ deg, the bar and measurement system are located close to the Spektr module surface, and there is possible interaction of the argon plume periphery with the OAA, whose density is comparable with the plume density at $\theta \ge 90$ deg.

Thus, further processing of results of the Astra-2 experiment should proceed in two directions. The first one is to obtain absolute pressure values. This requires the analysis of three-dimensional flow inside the pressure gauge for a wide range of rarefaction parameters. As it follows from Fig. 11, the plume density near the gauge varies by five orders of magnitude, depending on the angle θ. The second direction is to take into account argon condensation within the nozzle and the near vicinity (Navier–Stokes zone), for determining the plume parameters near the pressure gauge. It is also necessary to study the influence of argon molecules reflected on the bar and elements of the measurement system on the plume structure.

All of these efforts are currently in progress.

Conclusions

The present paper describes an experimental setup for measurements in the far field of the plume exhausted from a small argon thruster mounted on the module Spektr of the space station Mir. The measured angular pressure distribution in the plume far field is presented.

The flow in the nozzle, near vicinity, and far field of the plume was numerically studied on the basis of a multizone approach. A Navier–Stokes solver was used for flow calculations in the nozzle and near vicinity, and a DSMC code was used for the remaining region.

The applicability of well-known engineering point-source models for far-field descriptions is analyzed. It is shown that using the distributed point-source model approach and a proper starting surface, it is possible to achieve good agreement with DSMC results.

A comparison of numerical predictions and experimental data on angular distribution of the relative pressure in the far field of the plume shows that it is necessary to take into account the processes of argon condensation both inside the nozzle and in the near vicinity.

The present DSMC plume study is unique because it has been performed in the near continuum through transitional to free-molecular regime, and offers a good basis for improving the physical model of molecular collisions at very low temperatures.

Acknowledgments

The authors gratefully acknowledge support by the Russian Foundation for Basic Research, Grant 98-01-00677. Sokolov wishes to acknowledge Alexey A. Ignatiev of the Institute of High Performance Computing and Data Bases for his assistance in conducting the Navier–Stokes computations.

References

[1]Ivanov, M., Markelov, G., Kashkovsky, A., and Giordano, D., "Numerical Analysis of Thruster Plume Interaction Problems," *Proceedings of the 2nd European Spacecraft Propulsion Conference*, European Space Agency, The Netherlands, 1997, pp. 603–610.

[2]Giordano, D., Ivanov, M., Kashkovsky, A., Markelov, G., Tumino, G., and Koppenwallner, G., "Application of DSMC to the Study of Satellite Thruster Plumes," AIAA Paper 97-2538, June 1997.

[¶]Itkin, A. L., private communication.

[3]Kogan, N. M., *Rarefied Gas Dynamics*, Plenum, New York, 1969.

[4]Bird, G., *Molecular Gas Dynamics and the Direct Simulation of Gas Flows*, Clarendon, Oxford, England, UK, 1994.

[5]Ivanov, M. S., Antonov, S. G., Gimelshein, S. F., and Kashkovsky, A. V., "Rarefied Numerical Aerodynamic Tools for Reentry Problems," *Proceedings of the 1st European Computational Fluid Dynamics Conference*, Elsevier, New York, 1992, pp. 1121–1128.

[6]Gerasimov, Y. I., "Similarity Parameters in the Problem of Interaction of a Free Expanding Jet with a Plate," *Izvestiya Akademii Nauk SSSR, Seriya Mekhanika Zhidkosti i Gaza* (translated as *Fluid Dynamics*), Vol. 2, No. 2, 1981, pp. 169–173.

[7]Simons, G. A., "Effect of Nozzle Boundary Layers on Rocket Exhaust Plumes," *AIAA Journal*, Vol. 10, No. 11, 1972, pp. 1534, 1535.

[8]Narasimha, R., "Collisionless Expansion of Gases into Vacuum," *Journal of Fluid Mechanics*, Vol. 12, No. 1, 1962, pp. 294–308.

[9]Woronowicz, M. S., and Rault, D. F. G., "On Plume Flowfield Analysis and Simulation Techniques," AIAA Paper 94-2048, June 1994.

[10]Rault, D. F. G., "Methodology for Thruster Plume Simulation and Impingement Effects Characterized Using DSMC," AIAA Paper 95-2032, June 1995.